ELSEVIER

Journal of Power Sources 81–82 (1999) 448–453

JOURNAL OF POWER SOURCES

www.elsevier.com/locate/jpowsour

Lithium insertion behaviour of $Li_{1+x}V_3O_8$ with different degrees of crystallinity

Jin Kawakita *, Takahiro Kato, Yasushi Katayama, Takashi Miura, Tomiya Kishi

Department of Applied Chemistry, Faculty of Science and Technology, Keio University, Hiyoshi 3-14-1, Kouhoku-ku, Yokohama 223-8522, Japan

Abstract

Lithium insertion behaviour of amorphous $Li_{1+x}V_3O_8$ was compared with that of poorly crystalline and highly crystalline LiV_3O_8. This oxide retained the amorphous state during discharge and charge cycle and exhibited electrochemical performance inferior to the crystalline one, i.e., smaller discharge capacity and lower cycle efficiency. The crystallinity of the crystalline $Li_{1+x}V_3O_8$ was one of the primary factors determining the rate of lithium insertion reaction. © 1999 Elsevier Science S.A. All rights reserved.

Keywords: Amorphous; Vanadate; Quenching; Lithium; Insertion

1. Introduction

Lithium trivanadate, $Li_{1+x}V_3O_8$ is one of the attractive active materials for the positive electrodes of lithium secondary batteries. Since Besenhard and Schöllhorn [1] found the possibility of insertion of Li^+ ions to $Li_{1+x}V_3O_8$ from the non-aqueous electrolyte, many researchers have attempted to improve its electrochemical performance.

Nassau and Murphy [2] reported the larger discharge capacity of glassy $Li_{1+x}V_3O_8$ in early cycles and more rapid deterioration in subsequent cycles than crystalline one. They prepared glassy (or amorphous) and crystalline forms by quenching and slow cooling of the melt, subsequently Pasquali et al. [3] reported slight inferiority of amorphous to crystalline $Li_{1+x}V_3O_8$ during the first cycle and deterioration with cycling in terms of the capacity. Other techniques [4] were applied to reduce the particle size of crystalline form to obtain a larger capacity. In these days, the theoretical discharge capacity of LiV_3O_8 was estimated to be 279 mA h g^{-1}, assuming the accommodation of up to three equivalent of Li^+ ions per formula unit, i.e., $x = 3.0$ in $Li_{1+x}V_3O_8$.

Pistoia et al. [5] prepared amorphous $Li_{1+x}V_3O_8$ using sol–gel method. It had the larger discharge capacity (419 mA h g^{-1}: $x = 4.5$) and the longer retention of capacity in many cycles than crystalline oxide. West et al. [6] obtained $Li_{1+x}V_3O_8$ in a finely dispersed form by heat treatment and dehydration of aqueous lithium vanadate gels, resulting in a high capacity (372 mA h g^{-1}: $x = 4.0$) and good reversibility. However, the product obtained by this method may possess water molecules in the compound, which was reported to bring the favored result [7].

Therefore, the authors elucidated the characteristics of lithium insertion reaction of amorphous $Li_{1+x}V_3O_8$ without water molecules and the effect of morphology and crystallinity on the lithium insertion behaviour of $Li_{1+x}V_3O_8$. In this paper, crystallinity was classified into three types. The first is amorphous vanadate prepared by quenching of the melt, termed as AM. The second is low crystalline one obtained by heat treatment of the AM sample, termed as LC. The last is highly crystalline material prepared by slow cooling of the melt, termed as HC. The AM sample was compared with both the LC and HC samples in terms of insertion behaviour.

2. Experimental

$Li_{1+x}V_3O_8$ (AM) was prepared as follows. A mixture of lithium oxide (Li_2O, Soekawa Chemicals, > 99.9% purity) and vanadium pentoxide (V_2O_5) in molar ratio of 1.2:3 was heated in a platinum crucible at 900°C for 30 h in air. V_2O_5 used in this experiment was synthesized by thermal decomposition of ammonium metavanadate (NH_4VO_3, Soekawa Chemicals, > 99% purity) at 500°C for 24 h. The crucible was swung for some times to attain the homogeneous composition of the melt. Then, the melt

* Corresponding author. Tel.: +81-45-563-1141; Fax: +81-45-563-5967; E-mail: kawakita@chem.keio.ac.jp

0378-7753/99/$ - see front matter
PII: S0378-7753(99)00197-4

was quenched by putting the crucible on ice water rapidly. The resulting sample was ground and heated at 215 or 350°C for 12 h in air to produce the LC215 or LC350 sample. As the reference material, high crystalline $Li_{1+x}V_3O_8$ (HC) was prepared by the conventional high temperature synthesis [8]. Thermogravimetry and differential thermal analysis (TG-DTA, Mac Science TG-DTA 2000) were carried out on the AM sample to detect the transition from amorphous to crystalline state.

Electrochemical measurements were carried out by using the three-electrode cell described elsewhere in details [9]. The working electrode was prepared by mixing and pressing the mixture of the oxide, acetylene black (Denka Black, Denkikagaku Kogyo) and poly(tetrafluoroethylene) (PTFE, Mitsui-Du Pont) in a weight ratio of 70:25:5. Metallic lithium rods were used as the counter and reference electrodes. The electrolyte was 1 mol dm^{-3} lithium perchlorate/propylene carbonate solution ($LiClO_4$/PC, Mitsubishi Chemical, battery grade) containing water within 20 ppm. All the cells were fabricated in a glove box filled with argon gas. Galvanostatic discharge and discharge/charge cycle tests were performed with an aid of galvanostat/potentiostat (Toho Technical research PS-08). The rest potential was regarded as the quasi open circuit potential (OCP) when its change was within 0.001 V h^{-1} after discharge experiment.

The lithiated product was also prepared by the chemical method described elsewhere in detail [9]. The sample powder was dispersed in an *n*-BuLi/*n*-hexane solution and stirred at room temperature for 7 days under argon atmosphere. The lithium content of lithiated samples was determined by elemental analysis for Li and V using atomic absorption analysis (Hitachi, 180-55 AAS).

These vanadates before and after lithium insertion were examined by X-ray diffraction (XRD, Rigaku RINT 1300) by CuKα radiation with nickel filter, and (FT-IR, Bio-Rad FTS-165) spectroscopic measurements using KBr disk method.

3. Results and discussion

3.1. Preparation

Fig. 1 shows the TG-DTA curves of amorphous $Li_{1.2}V_3O_8$ (AM). Two exothermic peaks appeared at about 200 and 250°C on the DTA curve. A similar DTA curve was observed under N_2 atmosphere by Nassau and Murphy [2], who ascribed two peaks to the formation of crystalline LiV_6O_{15} and LiV_3O_8 phases, respectively. They did not, however, show any TG curves or XRD patterns. The TG curve in Fig. 1 did not have any weight change at this temperature range, though weight loss caused by vaporization of adsorbed water could be seen below about 150°C. As discussed below, XRD patterns of the samples heat treated at 215 and 350°C (see Fig. 2) were ascribed

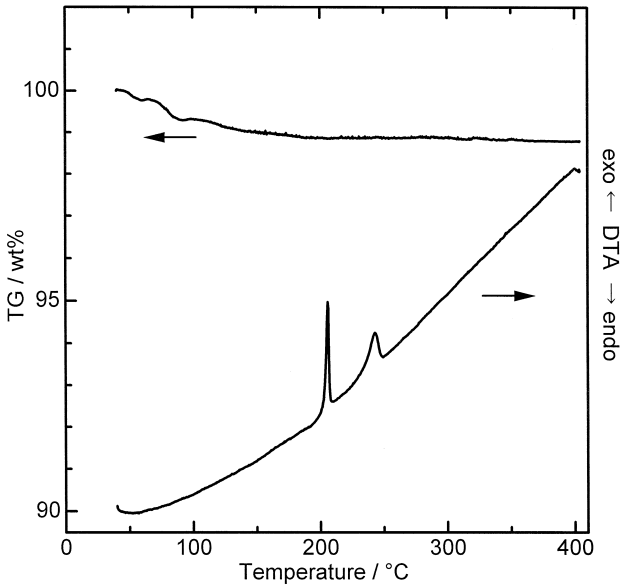

Fig. 1. TG-DTA curves of amorphous $Li_{1.2}V_3O_8$.

those of LiV_3O_8 (and had not any diffraction line ascribed to LiV_6O_{15}). These observations suggested that the two exothermic peaks at 200 and 250°C observed under air would be attributed to crystallization of LiV_3O_8 phase and to any ordering phenomenon described later.

Fig. 2 gives the XRD patterns of $Li_{1.2}V_3O_8$ (AM. LC215, LC350, and HC). No obvious diffraction lines appeared in the pattern except for a hallow characteristic of the amorphous substance, as shown in Fig. 2a. All the diffraction lines of the LC215 (with coexisting graphite marked by arrows), LC350 and HC samples were attributed to $Li_{1+x}V_3O_8$ (indexed in JCPDS card No. 18-754), as shown in Fig. 2b–d. The lattice parameters of these crystalline samples coincided well with the JCPDS data. Relative intensities of the diffraction lines of (020) and (003) to (100) for LC215 and LC 350 were similar to those of the JCPDS card, but stronger (100) diffraction line was observed for HC sample, as shown in Fig. 3. The latter may be caused by a preferred orientation of the crystal due to a plate-like shape of the HC powdered sample. The grain sizes, calculated from data of full width at half maximum using Scherrer's equation were 70–80, 25–32, 20–28 nm for HC, LC 350 and LC215, respectively, independent of the crystal directions. These results indicated the diffraction line broadening might be accounted as imperfection of the crystal rather than grain size, and LC samples might have some crystal disorders.

Fig. 4 shows the FT-IR spectra of $Li_{1.2}V_3O_8$ (AM, LC and HC). Referring to the previous studies on IR spectra of this oxide [10,11], the two main peaks around 1000 and 950 cm^{-1} were ascribed to the stretching vibration between V and O atoms, ν(V=O). Though these two peaks were observed obviously for the HC sample, they were broadened and overlapped for the LC sample, as seen in

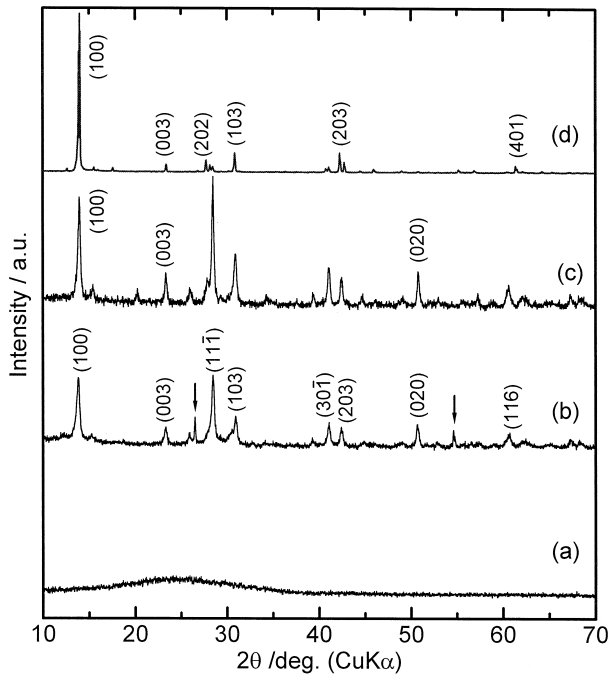

Fig. 2. XRD patterns of $Li_{1.2}V_3O_8$, (a) prepared by quenching (AM), heat treated at (b) 215°C (LC215) and (c) 350°C (LC350), and (d) prepared by slow cooling (HC).

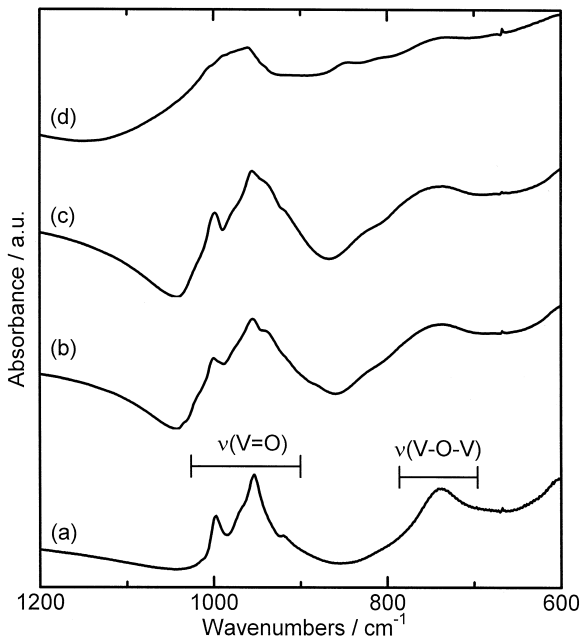

Fig. 4. IR spectra of $Li_{1.2}V_3O_8$, (a: HC, b: LC350, c: LC215, and d: AM).

Fig. 4a and b. A broad peak was observed near 950 cm^{-1} for the AM sample. These results indicated the existence of the short-range order of VO_6 unit in the HC sample, and increasing indistinct separation of these peaks for the LC and AM samples was due to increasing disorder of a regular configuration of the atoms. On the other hand, the peak near 730 cm^{-1} attributed to the stretching vibration between V and O atoms, ν(V–O–V), indicated the existence of the long-range order for the HC sample, as presented in Fig. 4a. This peak became ambiguous for the LC sample, and further for the AM sample. These disorders might appear as the diffraction line broadening in the XRD patterns. Relative integrated absorbance of the absorption band of ν(V–O–V) to that of ν(V=O) increased in order of the temperature of heat treatment, i.e., RC < LC350, the last of which has the relative absorbance similar to that of HC sample. This suggested that VO_6 units in the intralayer were arranged in more regular manner by heat treatment above 220°C where the second exothermic peak appeared. The broad exothermic peak at 220 to 250°C in the DTA curve (Fig. 1) will be related to an arrangement of the layer to gain some long-range orders.

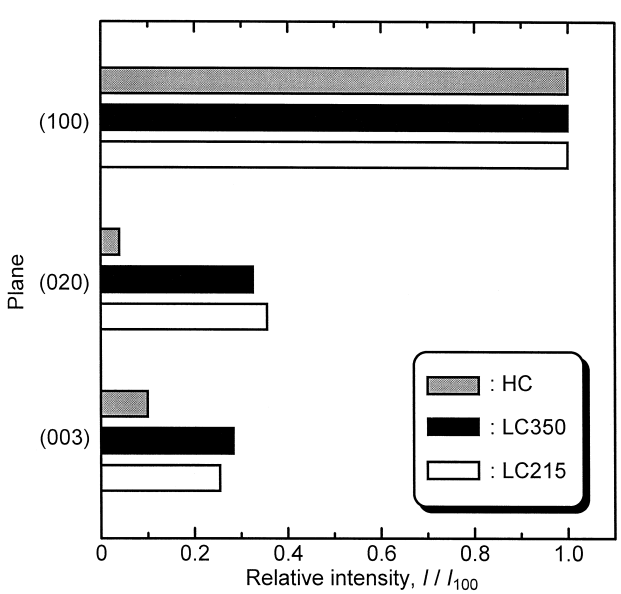

Fig. 3. Relative intensity in some planes of $Li_{1.2}V_3O_8$.

3.2. Lithium insertion behaviour

Fig. 5 shows an open circuit potential (OCP) of the oxides versus composition x in $Li_{1+x}V_3O_8$ obtained by electrochemical lithium insertion. The continuous decrease in the potential of the AM sample was characteristic of the amorphous material. On the other hand, the plateau of potential was observed near 2.6 V (vs. Li^+/Li) for the LC350, LC215 and HC samples. In this plateau, the original LiV_3O_8 phase and the second $Li_4V_3O_8$ phase coexisted [9]. Though the HC sample had the insertion limit at $x = 3.0$, further lithium insertion proceeded up to near $x = 4.0$ in the AM sample as well as the LC sample. The potential plateau at 2.4 V in the LC sample was also observed in LiV_3O_8 prepared by the sol–gel method and the subsequent heat treatment [6,12].

The XRD patterns of the fully lithiated by chemical method samples of $Li_{1+x}V_3O_8$ were compared in Fig. 6.

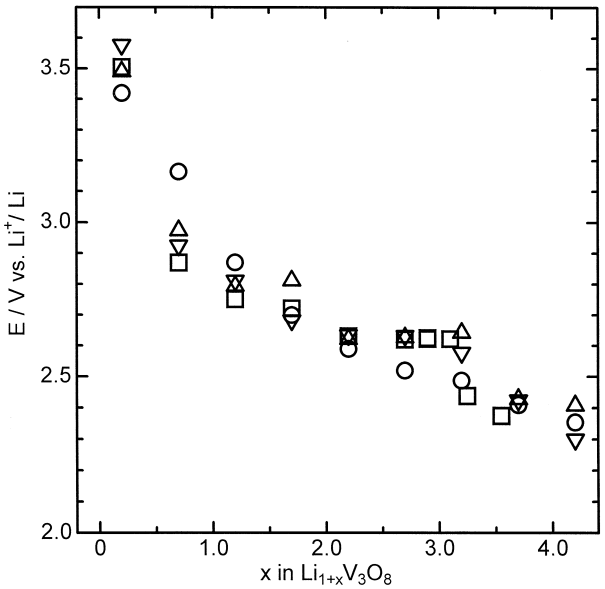

Fig. 5. OCP plots of $Li_{1+x}V_3O_8$, (○: AM, ▽: LC215, △: LC350, and □: HC).

As for both the LC and HC samples (Fig. 6a and b), all the diffraction lines in the patterns were ascribed to the phase found out by Picciotto et al. [13]. On the other hand, no diffraction lines in the pattern of the AM sample (Fig. 6a) showed the successive absence of the crystalline phase upon lithiation.

The IR spectra of the fully lithiated by chemical method samples of $Li_{1+x}V_3O_8$ were drawn as the solid lines and compared in Fig. 7. The dashed lines represented the respective unlithiated sample, $Li_{1.2}V_3O_8$. As seen in Fig. 7a and b, the assembling of the absorption bands from near 950 and 740 cm^{-1} to around 850 cm^{-1} was explained by a homogenization of the bond lengths due to the formation of the rock-salt type defect $Li_4V_3O_8$ [11]. In the case of the AM sample, the shifting of the band from near 950 cm^{-1} to the lower wavenumbers corresponded to the decrease of the bond strength between V and O atoms rather than homogenization of the bond lengths. This phenomenon was caused by the reduction of vanadium component to the lower valence state.

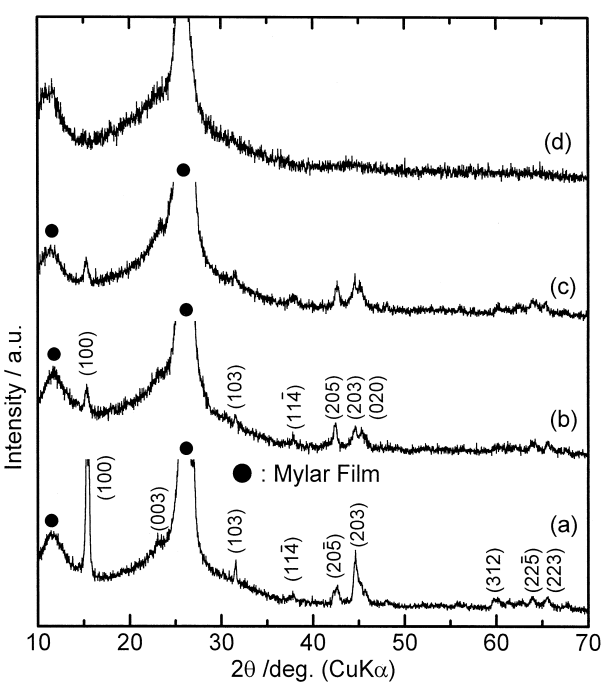

Fig. 6. XRD patterns of chemically lithiated samples, $Li_4V_3O_8$, (a: HC, b: LC350, c: LC215, and d: AM samples).

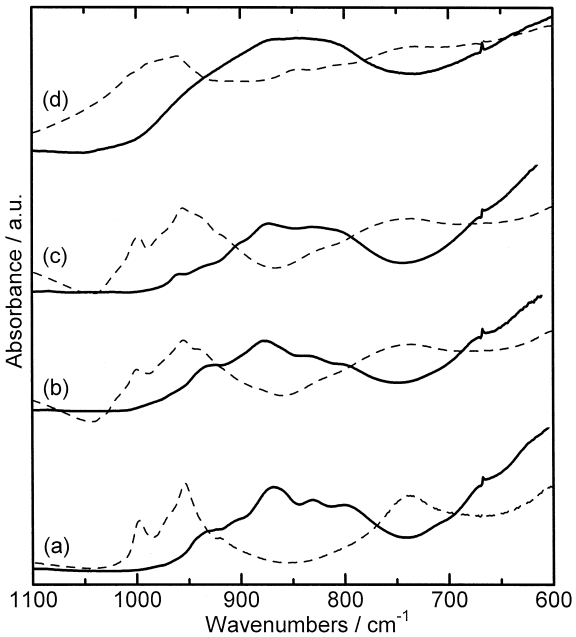

Fig. 7. IR spectra of chemically lithiated samples, $Li_4V_3O_8$, (a: HC, b: LC350, c: LC215 and d: AM).

3.3. Discharge and charge cycling characteristics

Fig. 8 shows the first discharge and charge cycle curves of the samples. Lithium insertion/extraction reaction of crystalline $Li_{1+x}V_3O_8$ less than 3.0 moles of Li^+ ions was reversible for HC sample [14]. Especially, each step in the discharge curve of the LC350 sample was observed wider and more obviously than for HC sample and at the corresponding plateau potentials during charging. In the case of the AM sample, on the contrary, the absence of any plateaus during discharging and charging indicated the absence of crystallization. The behaviour of LC215 was situated between LC350 and AM samples. These data indicated that a crystalline oxide is more feasible to lithium insertion than an amorphous oxide, though large and (100) preferential orientation of the HC oxide retarded lithium insertion. Moreover, the amorphous oxide had unextractable lithium upon charging.

The dependence of the discharge capacity on the current density were shown in Fig. 9a, where the first discharge and charge was cycled between 3.5 and 1.5 V. The discharge capacity decreased as the c.d. increased, and the

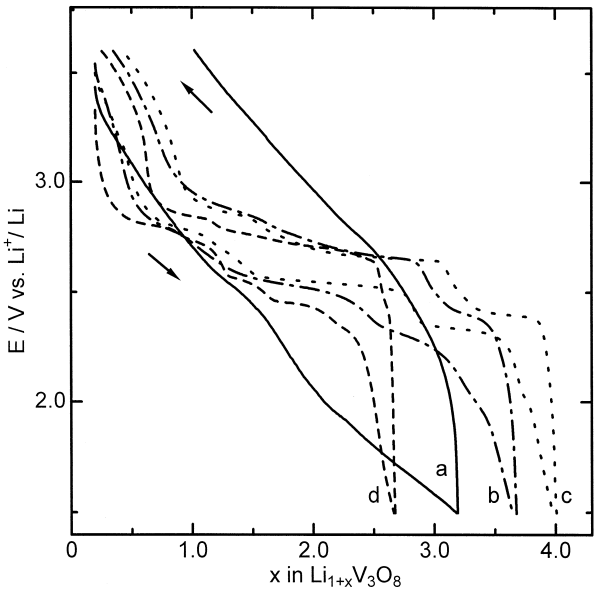

Fig. 8. Discharge and charge curves of $Li_{1.2}V_3O_8$ at ± 0.2 mA cm^{-2}, (a: AM, b: LC215, c: LC350, and d: HC).

capacity for LC350 was larger than that for LC215, due to a larger diffusivity for LC350 owing to more regular arrangement of the layered structure than for LC215. Differences in the capacity between LC and AM and HC samples, especially at larger c.d., were caused by lack of lithium insertion accompanied by the transition from LiV_3O_8 to $Li_4V_3O_8$ phase. Causes of the lack were a slow transition rate for the HC and an amorphous nature for the AM samples. Dependence of the coulombic efficiency of the first cycle on the current density was given in Fig. 9b. There was a tendency that the samples with amorphous

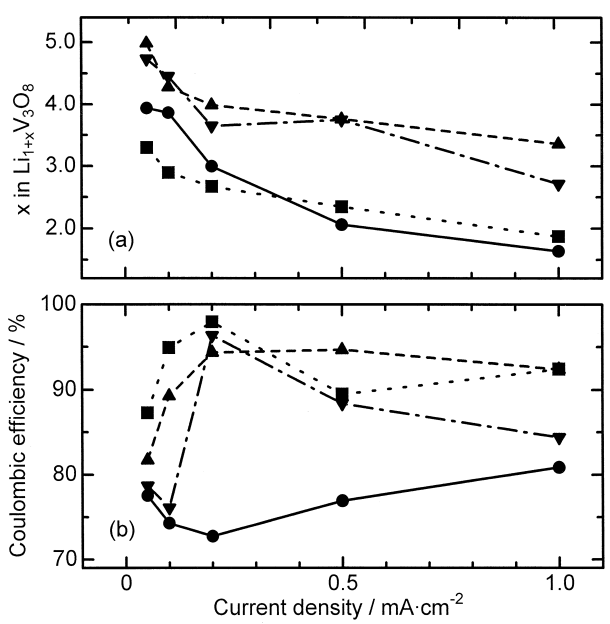

Fig. 9. Dependence of (a) x in $Li_{1+x}V_3O_8$ up to 1.5 V and (b) coulombic efficiency during first cycle between 3.5 and 1.5 V on current density, (●: AM, ▼: LC215, ▲: LC350, and ■: HC).

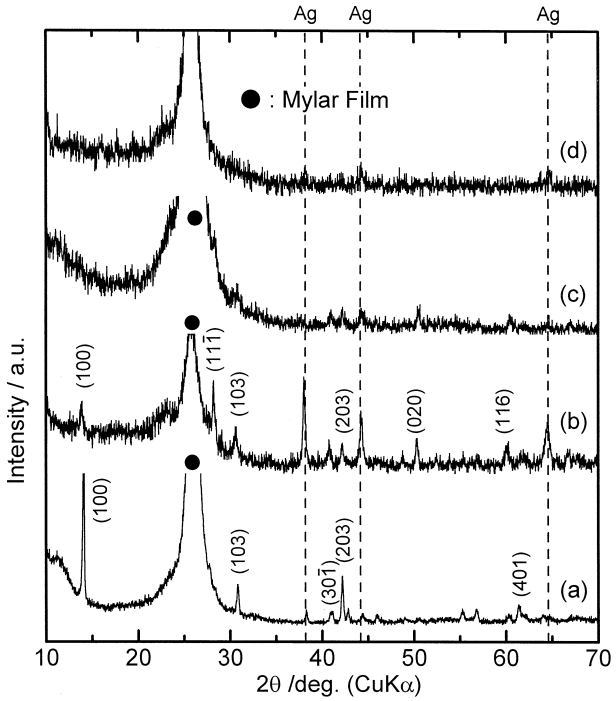

Fig. 10. XRD patterns of $Li_{1.2}V_3O_8$ after first cycle between 3.6 and 1.5 V, (a: HC, b: LC350, c: LC215, and d: AM).

nature (AM and partially LC215) had smaller efficiencies than crystalline ones. In crystalline $Li_{1+x}V_3O_8$, Li^+ ions residing in octahedral sites before lithium insertion act as a 'pin' of the layers and exert no hindrance over the incoming Li^+ ions occupying the empty tetrahedral sites [15]. Contrary to this, diffusion of Li^+ ions became slower in the AM sample so that preexisting Li^+ ions prevented inserted Li^+ ions from diffusion. Furthermore, an attractive interaction between inserted Li^+ and O^{2-} ions might have difficulty in lithium extraction from the AM sample during charging, leading to considerably lower efficiency than crystalline oxides.

Fig. 10 shows the XRD patterns of $Li_{1.2}V_3O_8$ (AM, LC, and HC) after first discharge and charge cycle between 3.6 V and 1.5 V. Note that the peaks overlapped with the dashed lines in the pattern were due to the existence of metallic silver (Ag) which was used for connecting a copper lead with a pellet of the working electrode and could not be washed out completely. As for the HC and LC sample (Fig. 10a and b, respectively), the reversible structural change from the $Li_4V_3O_8$ to LiV_3O_8 phase was found out, as the diffraction patterns before cycling appeared. On the other hand, no diffraction lines in the pattern of the AM sample resulted in keeping the amorphous state during charging as well as during discharge.

4. Conclusion

It was revealed that amorphous $Li_{1+x}V_3O_8$ obtained by quenching from the melt of Li_2O and V_2O_5 retained the amorphous state during lithium insertion and extraction.

The amorphous $Li_{1+x}V_3O_8$ was inferior to the crystalline samples with respect to the rate capability of lithium insertion reaction because the repulsive interaction between preexisting and inserted Li^+ ions in the amorphous one lead to slower diffusion of Li^+ ions in contrast to case of the crystalline one. Furthermore, the lower coulombic efficiency of the amorphous one during first discharge and charge cycle was explained by the existence of unextractable Li^+ ions which were bonded strongly with O^{2-} ions.

The insertion rate of the crystalline $Li_{1+x}V_3O_8$ was influenced largely by the rate of the transition between LiV_3O_8 and $Li_4V_3O_8$ phases, which is dependent on size and shape and also imperfection of the oxide crystals.

References

[1] J.O. Besenhard, R. Schöllhorn, J. Power Sources 1 (1976) 267.
[2] K. Nassau, D.W. Murphy, J. Non-Cryst. Solids 44 (1981) 297.
[3] M. Pasquali, G. Pistoia, V. Manev, R.V. Moshtev, J. Electrochem. Soc. 133 (1986) 2454.
[4] G. Pistoia, M. Pasquali, Y. Geronov, V. Manev, R.V. Moshtev, J. Power Sources 27 (1989) 35.
[5] G. Pistoia, M. Pasquali, G. Wang, L. Li, J. Electrochem. Soc. 137 (1990) 2365.
[6] K. West, B. Zachau-Christiansen, S. Skaarup, Y. Saidi, J. Barker, I.I. Olsen, R. Pynenburg, R. Koksbang, J. Electrochem. Soc. 143 (1996) 820.
[7] V. Manev, A. Momchilov, A. Nassalevska, G. Pistoia, M. Pasquali, J. Power Sources 54 (1995) 501.
[8] J. Kawakita, H. Katagiri, T. Miura, T. Kishi, J. Power Sources 68 (1997) 680.
[9] J. Kawakita, Y. Katayama, T. Miura, T. Kishi, Solid State Ionics 107 (1998) 145.
[10] Y. Kera, J. Solid State Chem. 51 (1984) 205.
[11] R. Tossici, R. Marassi, M. Berrettoni, S. Stizza, G. Pistoia, Solid State Ionics 57 (1992) 227.
[12] J. Kawakita, Y. Katayama, T. Miura, T. Kishi, Solid State Ionics 110 (1998) 199.
[13] L.A. de Picciotto, K.T. Adendorff, D.C. Liles, M.M. Thackeray, Solid State Ionics 62 (1993) 297.
[14] G. Pistoia, M. Pasquali, M. Tocci, R.V. Moshtev, V. Manev, J. Electrochem. Soc. 132 (1985) 281.
[15] G. Pistoia, S. Panero, M. Tocci, R.V. Moshtev, V. Manev, Solid State Ionics 13 (1984) 311.